Effective Models in Evaluating Radio Coverage on Single Floors of Multifloor Buildings

J. H. Tarng, *Member, IEEE,* and T. R. Liu

***Abstract*—An effective site-specific hybrid model is developed to predict the path loss and the effective radio coverage on single floors. The hybrid model, combined with a two-dimensional (2-D) model and an easy-to-use direct-transmitted ray (DTR) model, is incorporated with the building blueprint in usage. Both effects of the interior walls and the metallic objects such as whiteboards, bookcases, and standing air conditioners on radio propagation are considered. It is found that inclusion of metallic objects will enhance the performance of the model.**

***Index Terms*—Field strength measurement, indoor propagation modeling, radio coverage.**

I. Introduction

FOR PERSONAL communication networks (PCN's) and wireless local area networks (WLAN's) such as DECT, CT2, CT3, and UPDC, a high standard of radio coverage in an indoor environment is required [1], [2]. To achieve this standard, an easy-to-use and reasonably accurate propagation model is necessary to give a radio coverage prediction which can be employed to make planning and installation of these systems as easy and cheap as possible. Therefore, regardless the complicated indoor radio environment, there are still a number of researches on indoor radio propagation modeling recently [3]–[12]. These researches have developed both the empirically based statistical models [3]–[7] and theoretical models [8]–[12].

In this paper, a theoretical hybrid model, which combines a two-dimensional (2-D) ray-tracing model with a direct-transmitted ray (DTR) model, is developed to predict the radio coverage on single floors in multifloored buildings. There were several researches [1], [7]–[12] which dealt with the related subjects before.

In [8], the authors used absorbing screens to represent the excess loss in office and hallway environments. In [9], the authors have developed a site-specific model to predict propagation based on a building blueprint representation. The concept of effective building material properties is developed. The same authors have also developed empirical formulations to predict radio attenuation due to the soft partitions and concrete walls that wholly or partially blocks the direct path between the transmitter and the receiver [7]. With the formulations, a contour plot with equal path loss in 10-dB steps is illustrated for a single floor. In these researches, the effects of metallic objects such as file cabinets, bookcases, standing air conditioners, or whiteboards on radio propagation is not examined in detail. These metallic objects not only block the direct and direct-transmitted paths, but also give a mirror reflection. The former effect can produce shadow zones behind the objects and the latter one can lead to a stronger multipath interference at some areas. Therefore, the radio coverage will be affected by these metallic objects.

In our research, a site-specific hybrid model incorporated with the building blueprint is developed to compute radio path loss on single floors. Not only the positions of concrete walls, gypsum-board walls, and concrete pillars are plotted in the floor blueprint, but also the boundaries of metallic objects are portrayed in the blueprint. The metallic objects are white boards, cabinets, bookcases, or standing air conditioners. The hybrid model, which includes the 2-D ray-tracing model and the DTR model, is combined with a patched-wall model. The patched-wall model is employed to describe and shape the complicated indoor propagation environment by introducing patches of different sizes and dielectric constants [12]. These patches are used to represent one of the surfaces of walls, doors, windows, concrete pillars, or the metallic objects as mentioned. The dimension and dielectric constant of each patch are determined, respectively, by the physical size and the material of which it represents.

With our model, the path loss of radio propagation on a floor in a multifloored building is predicted with a reasonable accuracy. This is shown by comparing the predicted path loss with the measured data of 2.44 GHz at four measurement sites. The DTR model can provide an accurate prediction for the situation when the direct path is not existing [non-line-of-sight (NLOS) propagation], but the direct transmitted (refracted) path is. The rest of the paper is organized as follows. The hybrid propagation model is introduced in Section II. In Section III, the measurement setup and experimental sites are introduced. Comparison between the measured path loss and the computed one is also illustrated. The conclusion is drawn in the last section.

II. Hybrid Propagation Model

In our model, the geometric optic method is used to trace significant direct (if existing), reflected, transmitted, or refracted rays by which the source reaches specified received locations. Our effective hybrid model includes the 2-D ray-tracing model and the effective DTR model. For the NLOS propagation situation, the DTR model is used to trace and

Manuscript received July 15, 1996; revised May 15, 1997. This work was supported by the National Science Council of Taiwan under NSC project 85-2221-E-009-35.

The authors are with the Department of Communication Engineering, National Chiao-Tung University, Hsinchu, Taiwan, R.O.C.

Publisher Item Identifier S 0018-9545(99)01028-2.

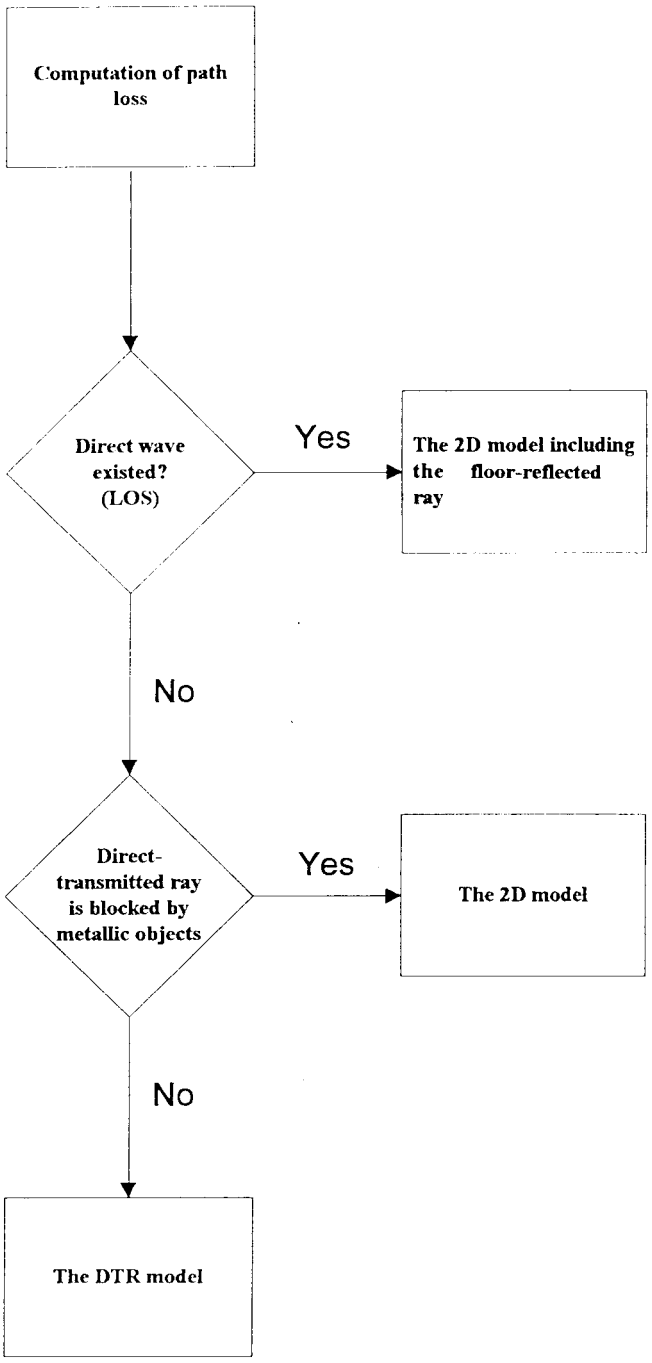

Fig. 1. The flow chart of the hybrid model to choose a proper model to compute path loss.

compute the direct-transmitted field when it is not blocked by metallic objects. In other propagation situations the received field strength will be computed by the 2-D ray-tracing model which may include the floor-reflected ray for line-of-sight (LOS) propagation. The ceiling-reflected ray is neglected since the ceiling is usually defined by support beam, pipes, ventilation ducts, lighting fixtures, etc., and act as scattering obstacles to the radio propagation. The scattered fields from the ceiling help to determine the interference pattern in the vicinity of the obstacles, but do not significantly affect the local average [9]. In Fig. 1, a flow chart shows how the hybrid model chooses a proper model in computing the path loss in various propagation situations. The purpose to identify the DTR model along, which can be incorporated into the 2-D model, is to explore whether the direct-transmitted ray (if it exists) is the dominant path in NLOS propagation situation. The model is also easy to implement and saves computation time.

A. Ray Tracing Technique

The ray tracing technique is used to trace the significant propagation paths from a transmitter location to a receiver location. The ray tube is introduced to represent the transmitting unit sphere. Each ray tube, chosen to have nearly equal shape and area, is represented by a source ray during the tracing process. The ray tracing is accomplished by an exhaustive search of a ray tree accounting for the decomposition of the ray at each building–object intersection. Initially, the algorithm verifies whether the LOS ray between the transmitter and the receiver is existing. Next, the algorithm traces a source ray along a predetermined direction and detects if the ray intersects with the boundary of an object. If no intersection is found, the process stops and a new source ray is initiated. Once an intersection has occurred, it then checks to see if the ray from the intersection point directly to the receiver is received. If this ray is not received, the ray is divided into reflected and transmitted (refracted) rays. This reflected or transmitted ray is then treated in a similar fashion as a source ray. This recursion continues until the ray intensity falls below a specified threshold or no farther intersections occur or the ray exceeds the binary tree chosen level. The reception sphere [8], [9] is also used to determine whether the traced ray approaching to a receiving point is received. Here, the reception sphere radius is equal to $\alpha d/2$, where d is the unfolded total path length and α is the angular spacing between neighboring rays at the source.

B. Reflection and Transmission Coefficients of Layered Media

Since in the real world the wall or floor in building has layered structure, a layered structure is considered in the computation of the transmission or reflection coefficient in our model. By treating each layer as a segment of transmission line with corresponding impedance, the transmission and reflection coefficients of the layered structure are calculated by $ABCD$ matrix and given by [13]

$$R_{s,p} = \frac{A + B/Z_t - Z_l(C + D/Z_t)}{A + B/Z_t + Z_l(C + D/Z_t)} \tag{1}$$

$$T_{s,p} = \frac{2}{A + B/Z_t + Z_l(C + D/Z_t)} \tag{2}$$

where the subscripts of s and p represent the incident wave with s (perpendicular) and p (parallel) polarizations, respectively. The notations A, B, C, D are computed by

$$\begin{bmatrix} A & B \\ C & D \end{bmatrix} = \begin{bmatrix} A_1 & B_1 \\ C_1 & D_1 \end{bmatrix} \begin{bmatrix} A_2 & B_2 \\ C_2 & D_2 \end{bmatrix} \cdots \cdots \begin{bmatrix} A_N & B_N \\ C_N & D_N \end{bmatrix}. \tag{3}$$

The coefficient in each matrix on the right-hand side of the equation above is determined by dielectric constant, permeability, layered thickness, and refractive angle of the corresponding layer. For example, for layer m

$$A_m = D_m = \cos q_m l_m$$
$$B_m = jZ_m \sin q_m l_m, \qquad (m = 1, \cdots, N) \tag{4}$$
$$C_m = \frac{j \sin q_m l_m}{Z_m}, \qquad A_m D_m - B_m C_m = 1 \tag{5}$$
$$q_m = k_m \cos\theta_m = k\left[1 - \left(\frac{n_l}{n_m}\right)^2 \sin^2\theta_i\right]^{1/2},$$
$$k_m = k_0 \cdot n_m \tag{6}$$

where θ_m is the refractive angle. Notation l_m is the layer thickness and n_m is the index of refraction. It is given that

$$q_i = k_l \cos\theta_i, \qquad q_t = k_t \cos\theta_t \tag{7}$$

where θ_i and θ_t are the angles of incidence at the initial layer and refraction at the final layer, respectively. It is noted that $Z_m = (\omega\mu_m/q_m)$ for s polarization and $Z_m = (q_m/\omega\varepsilon_m)$ for p polarization.

C. Two-Dimensional Propagation Model

The model includes direct, reflected, and transmitted fields that are represented by the rays. Each propagation mechanism is treated separately. The complex field of ith ray at the receiver is given by

$$E_i = E_0 \cdot G_{ti} \cdot G_{ri} \cdot L_i(d) \cdot \prod_j R(\theta_{ji}) \cdot \prod_m T(\theta_{mi}) \tag{8}$$

where E_0 is the field strength 1 m away from the transmitting antenna, G_{ti} and G_{ri} are the field-amplitude radiation patterns of the transmitting and the receiving antennas, respectively, and $L_i(d)$ is the free-space path loss of ith component with path length d. The reflection coefficient R and transmission coefficient T are given by (1) and (2), respectively. θ_{ji} and θ_{mi} are the jth reflecting and mth transmitting angles, respectively. It is noted that the received floor-reflected ray is also computed by (8) by setting $T(q_{mi}) = 1$.

D. DTR Model

In this model, a direct-transmitted (-refracted) ray (if existing) is traced and used to compute the average path loss for NLOS propagation. This direct-transmitted ray can be experienced transmission or refraction more than once before it is received. The received complex field is given by

$$E_R = E_O G_t G_r L(d) \prod_i T(\theta_i) \tag{9}$$

where G_t and G_r are the field-amplitude radiation gains at the direction of the direct-transmitted ray of the transmitting and the receiving antennas, respectively. $L(d)$ is the free-space path loss with path length d. The transmission coefficient $T(\theta_i)$ with incident angle θ_i is calculated by (2).

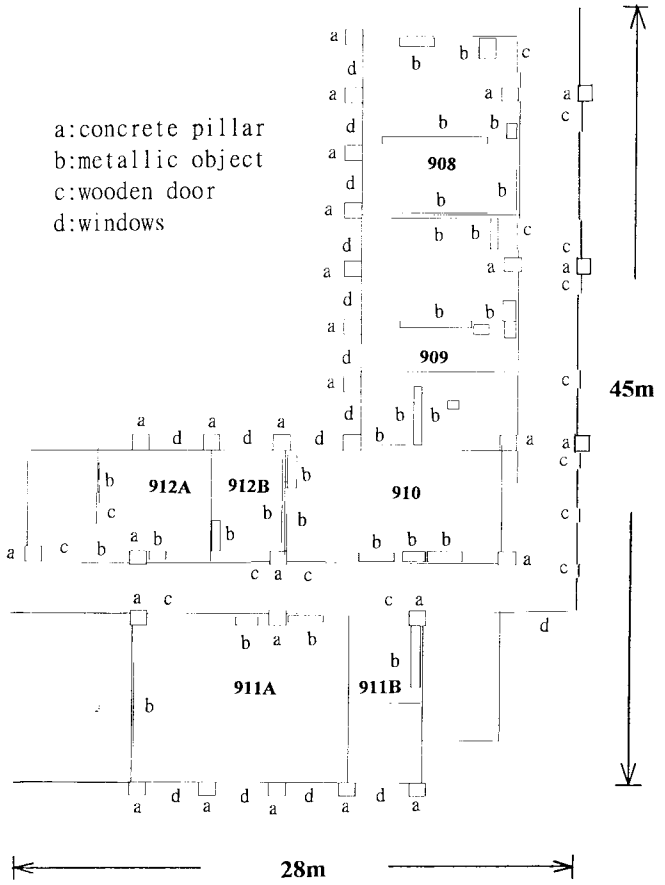

Fig. 2. The south and west wings of the floor plan blueprint where there are five measurement sites chosen. The metallic objects, such as cabinets, bookcases, standing air conditioners, and whiteboards, are also included.

III. Comparison with Measurements

A. Measurement Setup and Procedure

Narrow-band (CW) signal strength measurements were made at 2.44 GHz. A 0- or 13-dBm CW signal was transmitted by a half-wavelength dipole antenna at a height 1.6 m above the ground. The transmitting system—including a signal generator, a section of cable, and the transmitting antenna—has been calibrated in an anechoic chamber to measure the 1-m transmitting field strength in free space. The receiving antenna is also a half-wavelength dipole antenna (MP663A) with the same height. Both the transmitting and receiving antennas are vertically polarized during the measurement. The receiver (Advantest R3261A) can instantaneously measure the signal strength among 0 to -100 dBm over a 10 kHz for 2.44 GHz. The received data is acquired automatically by a personal computer with a GPIB card. At each measured position, the measured field strength is obtained by a spatial sector averaging over nine grid subpoints with a quarter wavelength spacing between neighboring subpoints. The main parameter of the measurement is the average field strength. The size of the sampled area should produce the parameter with a reasonable approximation. The size of the sampled area is determined by the spatial correlation length of the environment. When

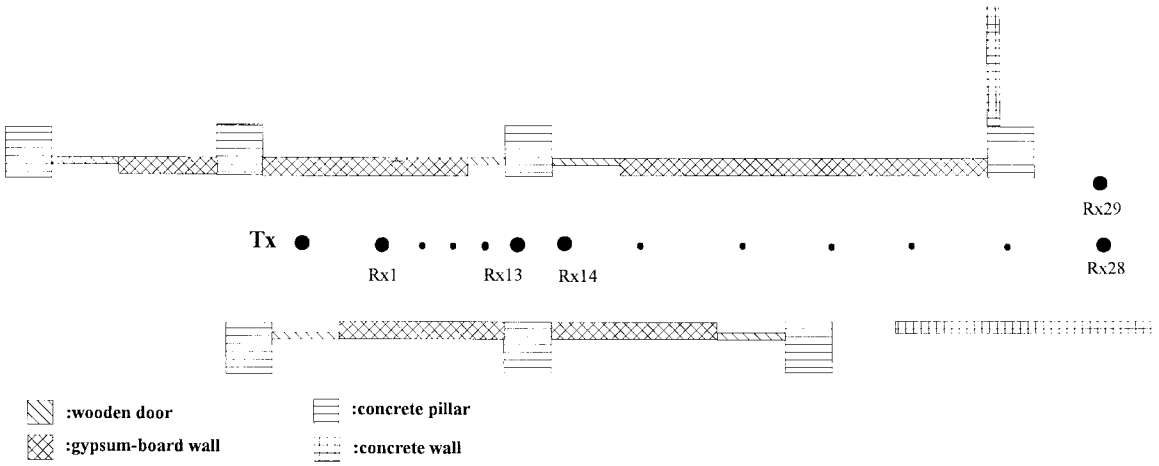

Fig. 3. Measurement site 1 is described by the patched-wall model. Tx and Rxi represent the positions of the transmitting and receiving antennas, respectively, with $i = 1, \cdots, 29$.

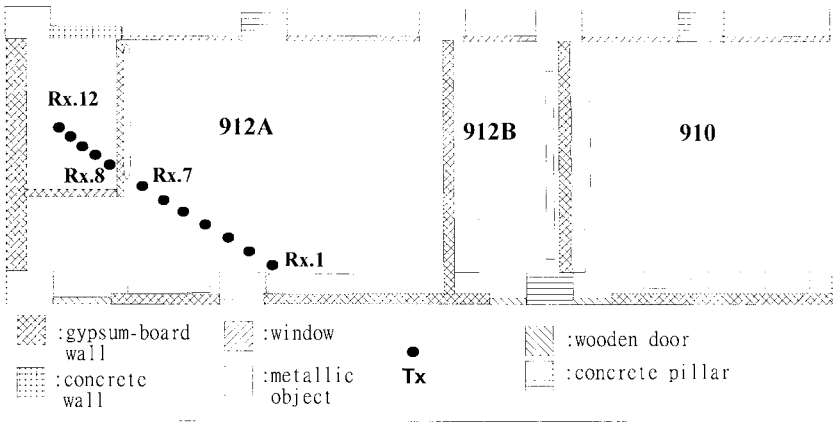

Fig. 4. Measurement site 2 is described by the patched-wall model. Six kinds of patch are used.

the distance between two sampled subpoints is larger than the correlation length, there two subpoints is treated as irrelevant and should not be included together to compute the averaged field strength. For indoor environments the spatial correlation length, which is much smaller than that of outdoor environments, is about $0.75\sim 1\lambda$ shown in [14] and [15], which is similar as the sampled size choose here. To ensure that the propagation channel is time stationary during the measurement, the measured data has been averaged on screen over ten instantaneous sampled data.

B. Experimental Sites

There are seven measurement sites that are all located at ninth floor of Engineering Building Four at the National Chiao-Tung University in Hsin-Chu. Building blueprint of ninth floor is shown in Fig. 2. The metallic objects, such as cabinets, bookcases, standing air conditioners, and whiteboards are also included and shown in the blueprint. To verify the 2-D and DTR models separately, the positions of the receiving antenna are properly arranged to produce three kinds of propagation situation depending on whether the direct-path or the directed-transmitted path between the transmitting and receiving antennas is existing. Fig. 3 shows measurement site 1. The receiving antenna is moving along a hallway while the transmitting antenna is fixed. The direct path is existing (situation 1). To describe the hallway properly, four kinds of patch are used to represent wooden doors, gypsum-board walls, concrete pillars, and walls separately as shown in Fig. 3. Fig. 4 shows measurement site 2. In this measurement, the direct path is not existing and the direct-transmitted path for every receiving position is blocked by metallic objects (situation 2) such as bookcases and air conditioners. Four rectangular metallic patches are used to form the surfaces of each metallic object. Measurement site 3 is shown in Fig. 5. In these measurements, although the direct path is blocked by the wall, the direct-transmitted path is existing (situation 3). At measurement sites 2 and 3, the patched-wall model is also used to shape the surface boundaries of the walls and metallic objects in the propagation environments. The concrete pillar is treated as a hollow post and each facet of the pillar is modeled as a patch with a finite thickness. A total number of 250 patches with six kinds are used.

C. Comparison of Path Loss

In the numerical simulation made with the 2-D model, a total of 720 source rays are generated and traced. The dielectric

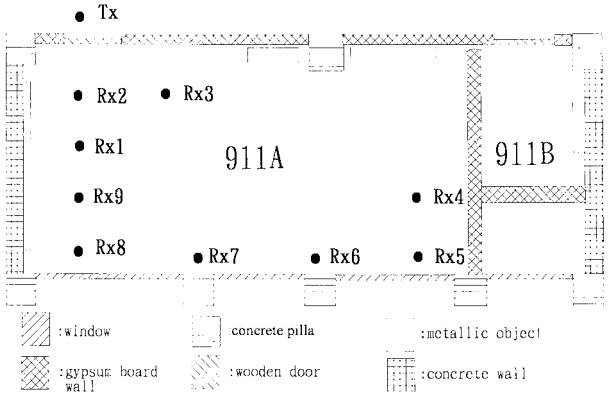

Fig. 5. Measurement site 3 is described by the patched-wall model. Six kinds of patch are used.

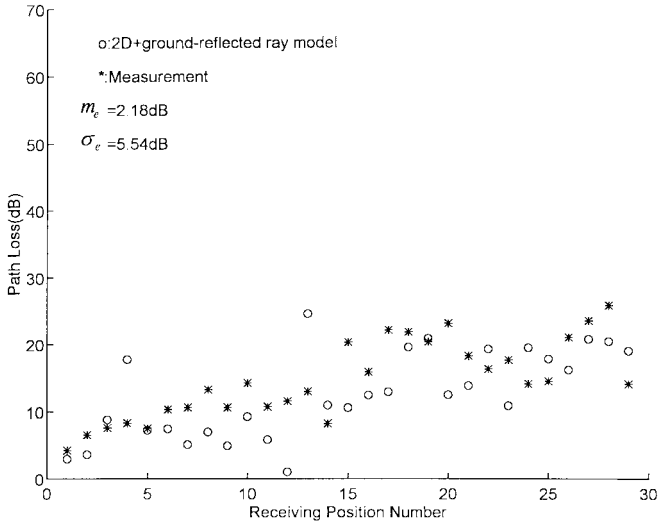

Fig. 6. The measured and predicted path losses of 2.44-GHz radio wave as a function of the receiving position number at measurement site 1.

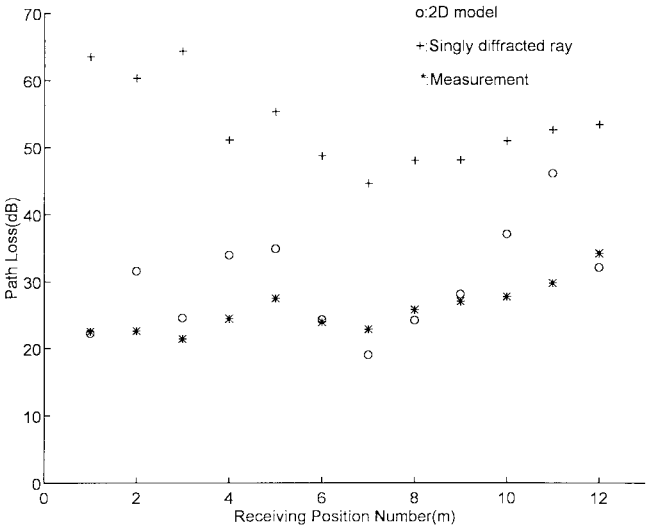

Fig. 7. The measured and predicted path losses of 2.44-GHz radio wave of the receiving positions at measurement site 2. Propagation loss of the singly diffracted path is also computed.

constants of gypsum-board walls, wooden doors, concrete walls, and ground floors are chosen to equal $5-0.062j$, $5-0.062j$, $7-0.6j$, and $7-0.6j$, respectively [16], [17]. At site 1, the path loss computed by the 2-D model plus the floor-reflected ray is compared with the measured one as shown in Fig. 6. It is found that the 2-D model plus the ground-

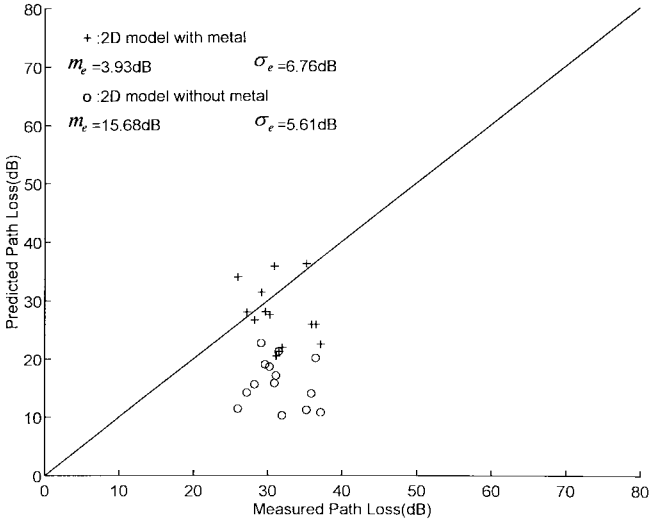

Fig. 8. The scatter plot of the measured versus predicted path loss for site 2. the sampled field strength is calculated by neglecting metallic objects which block the directed-transmitted ray.

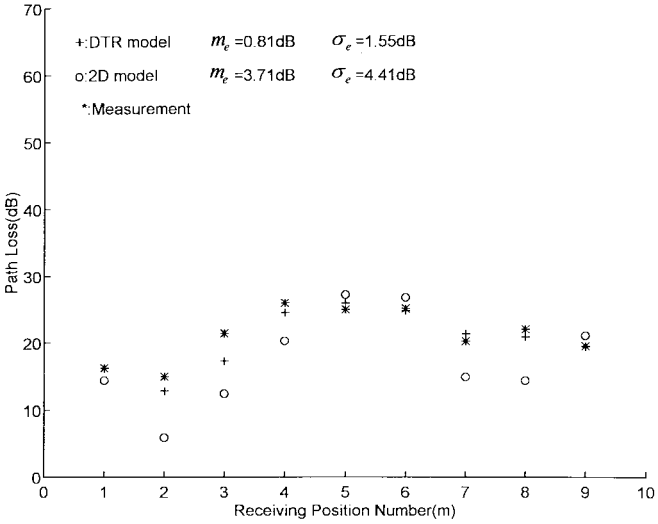

Fig. 9. The measured and predicted path losses of 2.44-GHz radio wave of the receiving positions at measurement site 3. Both the DTR and 2-D models are used.

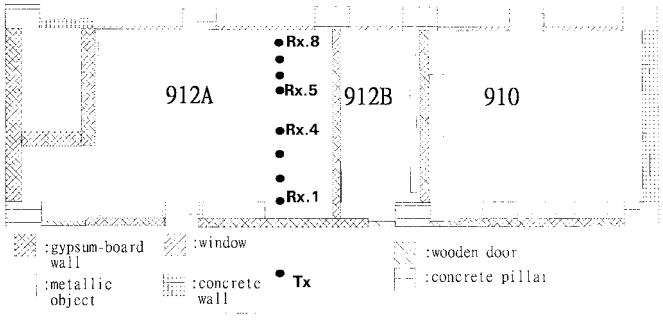

Fig. 10. Measurement site 4 is described by the patched-wall model.

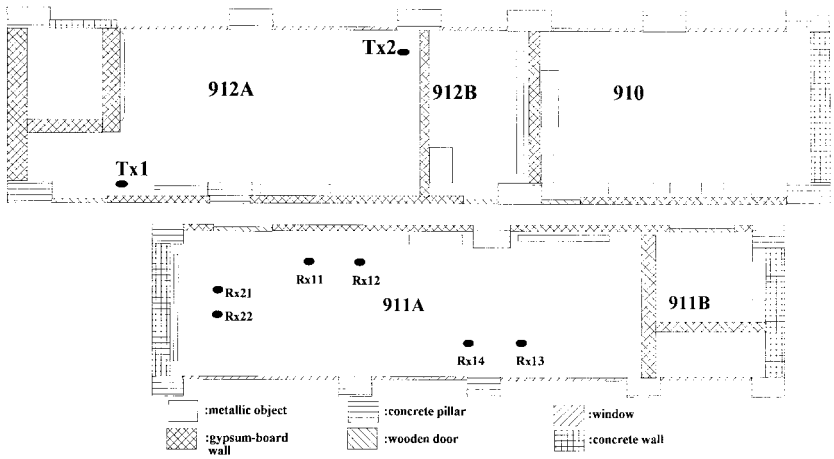

Fig. 11. Floor layout of measurement site 5 is shown by the patched-wall model. Experiments of the transmitter positions at Tx1 and Tx2 are carried out.

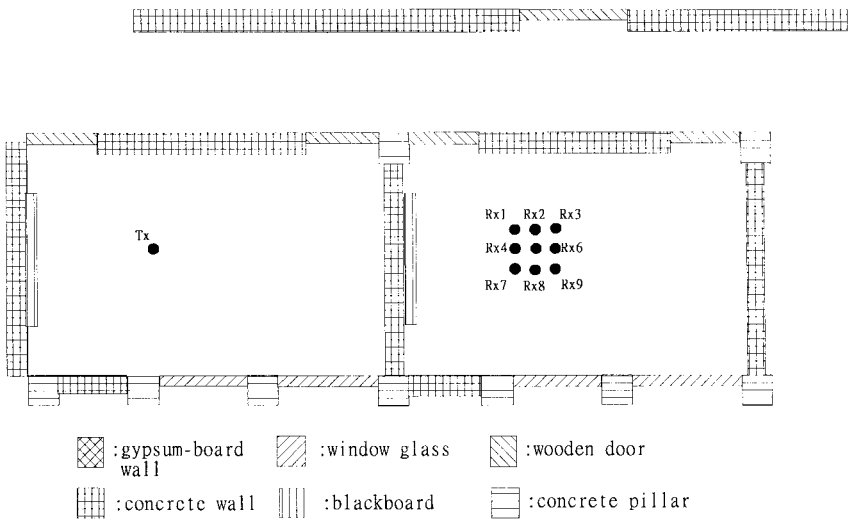

Fig. 12. Floor layout of measurement site 6 is shown by the patched-wall model.

reflected ray gives a reasonable prediction accuracy for 2.44 GHz radio propagation along the hallway (LOS propagation) with $m_e = 2.18$ dB and $\sigma_e = 5.54$ dB. Here, m_e represents the mean of the error and σ_e is the standard deviation of the error. Since both the direct and the direct-transmitted paths are not existing at measurement site 2, the predicted path loss computed by the 2-D model is compared with the measured one as shown in Fig. 7 to yield $m_e = -4.00$ dB and $\sigma_e = 5.87$ dB. At measurement site 2, the ray diffracted by the corner of metallic objects is not neglected since contribution from the singly diffracted rays is much smaller than that from the transmitted-reflected rays. It is observed in Fig. 7 that at measurement site 2 the path loss of singly diffracted ray is much larger than that predicted by the 2-D model at most of the receiving positions. Multiple reflections are the dominant propagation mode for this situation. To show the importance of including the metallic objects, a scatter plot of the measured versus predicted data for site 2 is illustrated in Fig. 8. One of the predicted data is calculated by neglecting the metallic object which blocks the directed transmitted ray. Including the directed transmitted ray, which is not existing, leads to an underestimation of the path loss and to an increase of σ_e, compared with the predicted data including the metallic object.

At measurement site 3, the DTR model is used to compute the path loss since the direct-transmitted ray is existing. Both the computed and measured path losses are illustrated in Fig. 9. It is found that the predicted result is very close to the measured one with $m_e = 0.81$ dB and $\sigma_e = 1.55$ dB. It shows that the DTR model gives an accurate prediction for the situation when the direct-transmitted ray is existing. It is noted that in Fig. 9 the 2-D model is also used to compute the path loss. It is found that although the 2-D model may include some extra transmitted-reflected rays as the received rays, it does not give a better prediction accuracy to compare with that of the DTR model. The comparison not only shows that the direct-transmitted ray is the dominant propagation mode, but also reveals a possibility that the reception sphere used in the 2-D model may receive some multiply transmitted-reflected rays which should not be included. It is because these rays are actually blocked, scattered, or attenuated by those objects been disregarded or simplified in the floor layout. Those objects include irregular walls, desk, chairs, etc.

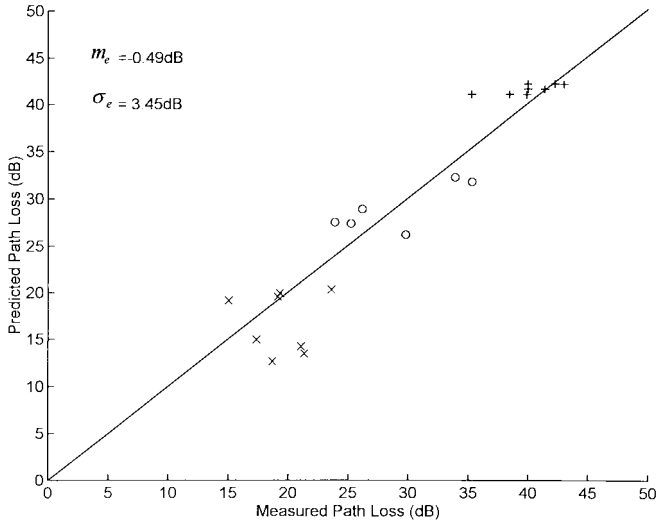

Fig. 13. The scatter plot of measured versus predicted path losses for all measured points at sites 4–6.

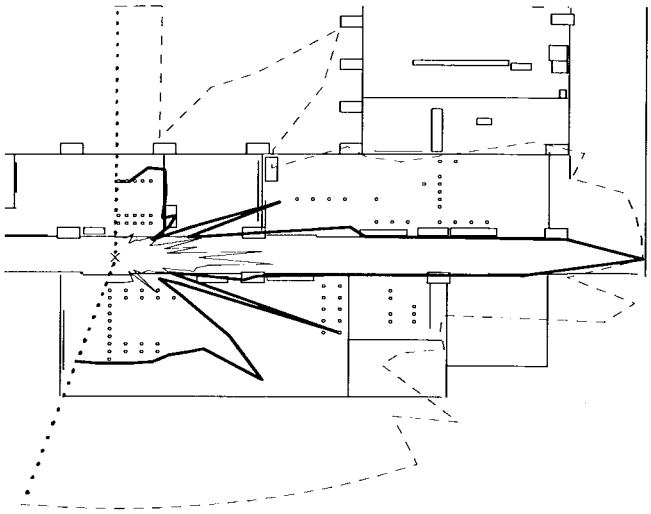

Fig. 14. The floor plan of measurement site 7. The patched-wall model is also used, but is not shown in detail. Contour plot for effective radio coverage is also shown.

With the simplification of the propagation environment, some additional rays or overweighed rays will be received and may cause an inaccurate prediction. It reflects a facet that a more sophisticated model requires more detail information of the propagation environment to yield a better performance.

Three other sites as shown in Figs. 10–12 are chosen to carry out the NLOS measurement of field strength, and the scatter plot of the measured versus predicted data is shown Fig,13. Notation "×", "◯", and "+" represent the data for sites Nos. 4–6, respectively. Since the direct-transmitted ray is not blocked by the metallic objects in these NLOS measurement, the DTR model is employed to predict the field strength and still yields a consistent predication accuracy with overall $m_e = -0.49$ dB and $\sigma_e = 3.45$ dB.

To assure the prediction accuracy of our hybrid model, other 75 receiving positions are measured at site 7 and their locations are shown by the small circle in Fig. 14. A scatter plot of the measured versus predicted data is shown in Fig. 15 and the hybrid model still gives a consistent prediction accuracy with $m_e = 2.01$ dB and $\sigma_e = 4.65$ dB.

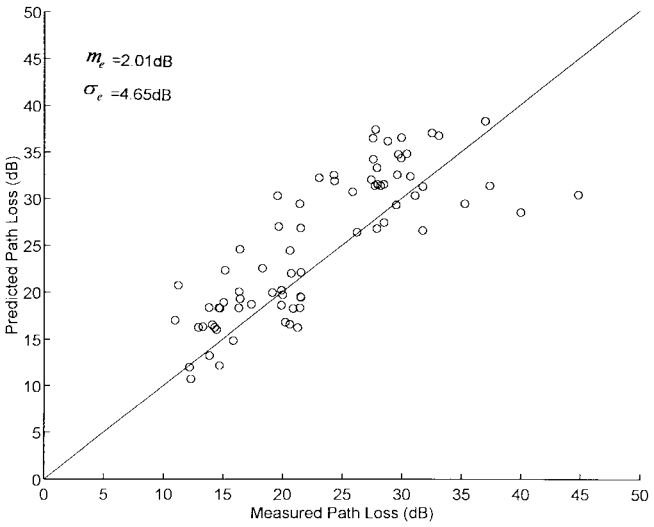

Fig. 15. The measured and predicted path losses of 2.44-GHz radio wave of the receiving positions at measurement site 7. The hybrid model is employed.

D. Radio Coverage Contour

The radio coverage contour, which is defined as the contour plotted with equal path loss, has been computed by using empirical formulations in [7]. In their approach, the contour is easy to determine since the path loss is only a log function, a one-to-one function, of propagation distance plus the excess loss due to the blockage of soft partitions and concrete walls. In our investigation, the field strength in the indoor environment, which is predicted by the theoretical hybrid model, oscillates along each receiving route because of multipath interference. The field strength that is equal to a specified value may be found in several positions along receiving route. The one-to-one mapping is not existing anymore. Hence, an alternative definition for radio coverage is required so that the one-to-one mapping is held and the radio coverage contour can be determined and plotted. Here, a concept of effective radio coverage contour is proposed and an effective contour expressed by $C(PL, \alpha)$ is introduced. The path loss of every position in the area enclosed by contour C is smaller than a chosen threshold value PL with probability α, i.e., the field strength in the contour is higher than a specified (threshold) value with probability α. The effective contour is formed by connecting neighboring contour points. The contour point on each radial axis originated from the transmitting point where the field strength within the range between the transmitting point and this specific point is higher or equal to the threshold value with probability α. The angular spacing between neighboring radial axes is the same. Here, the spacing between neighboring replaced point along each radial axis is equal to a quarter wavelength and the computed range is determined by the maximum physical dimension of the environment.

In Fig. 14, three effective radio contours are expressed by solid line, heavy solid line and dash line to represent PL = 10,

20, and 35 dB, respectively. In the computation, the coverage to the left area is limited by the dotted line and α is chosen to equal 80%. The major reason to choose the value of α as 80% is to demonstrate an identifiable radio contour, although it can be chosen as any value to fulfill the requirement of system design. The effective contour with a larger value of PL is smoother than that with a smaller value. This means that the cell shape with larger path loss is not so irregular even with a lot of metallic obstacles inside the cell. Although the metallic obstacles may block the direct and direct-transmitted rays and produce shadow areas, part of these shadow areas may be lightened due to the contribution from other multiply transmitted-reflected rays and yields a less irregular cell shape. Due to the guiding effects of the hallway, the cell can cover the area along the hallway effectively with the transmitting antenna being located somewhere in the hallway.

IV. Conclusion

In this research, it has been identified that the direct-transmitted ray is the dominant path in the evaluation of the mean path loss for NLOS propagation on single floor if the direct-transmitted path is not blocked by the metallic objects. In this situation, the easy-to-use DTR model combined with the patched-wall model is employed and gives an effective and accurate prediction. In other propagation situations, the 2-D ray-tracing model with inclusion of the ground-reflected ray can provide a reasonable prediction accuracy. The effective radio coverage contour is evaluated by using the hybrid model combined with a statistical approach. On a single floor, the effective contour with larger value of path loss is smoother than that with a smaller value.

References

[1] A. J. Motley and J. M. P. Keenan, "Radio coverage in buildings," *Brit. Telecom. Tech. J. (Special Issue on Mobile Commun.)*, vol. 8, pp. 19–24, 1990.

[2] M. Marcus, "Regulatory policy considerations for radio local area networks," *IEEE Commun. Mag.*, vol. 25, pp. 95–99, July 1987.

[3] T. S. Rappaport, "Characterization of UHF multipath radio channel in factory buildings," *IEEE Antennas Propagat.*, vol. 37, pp. 1058–1069, Aug. 1989.

[4] R. Bultitude, S. Mahmoud, and W. Sullivan, "A comparison of indoor radio propagation characteristics at 910 MHz and 1.75 GHz," *IEEE J. Select. Areas Commun.*, vol. 7, pp. 20–30, Jan. 1989.

[5] J. F. Lafortune and M. Lecours, "Measurement and modeling of propagation losses in a building at 900 MHz, " *IEEE Trans. Veh. Technol.*, vol. 39, pp. 101–108, May 1990.

[6] S. Y. Seidel and T. S. Rappaport, "Path loss prediction in multifloored buildings at 914 MHZ," *Electron. Lett.*, vol. 27, pp. 1384–1387, July 1991.

[7] S. Y. Seidel and T. S. Rappaport, "914 MHz path loss prediction models for indoor wireless communications in multifloored buildings," *IEEE Trans. Antennas Propagat.*, vol. 40, pp. 207–217, Feb. 1992.

[8] _____, "Site-Specific propagation prediction for wireless in-building personal communication system design," *IEEE Trans. Veh. Technol.*, vol. 43, pp. 879–892, Nov. 1994.

[9] W. Honcharenko, H. L. Bertoni, J. L. Dailing, J. Qian, and H. D. Yee, "Mechanisms governing UHF propagation on single floors in modern office buildings," *IEEE Trans. Veh. Technol.*, vol. 41, pp. 496–504, Nov. 1992.

[10] G. M. Whitman, K. S. Kim, and E. Niver, "A theoretical model for radio signal attenuation inside buildings," *IEEE Trans. Veh. Technol.*, vol. 44, pp. 621–629, Aug. 1995.

[11] A. Kajiwara, "Line-of-sight indoor radio communication using circular polarized waves," *IEEE Trans. Veh. Technol.*, vol. 44, pp. 487–493, Aug. 1995.

[12] J. H. Tarng, W. R. Chang, and B. J. Hsu "Three-dimensional modeling and measurement of 900 and 2.44-GHz radio propagation in corridors," *IEEE Trans. Veh. Technol.*, vol. 46, pp. 519–527, May 1997.

[13] A. Ishimaru, *Electromagnetic Wave Propagation, Radiation, and Scattering*. Englewood Cliffs, NJ: Prentice-Hall, 1991.

[14] G. E. Corazza, V. Degli-Esposti, M. Frullone, and G. Riva, "A characterization of indoor space and frequency diversity by ray-tracing modeling," *IEEE J. Select. Areas Commun.*, vol. 14, pp. 411–419, 1996.

[15] J.-F. Lemieux, M. S. El-Tanany, and H. M. Hafez, "Experimental evaluation of space/frequency/polarization diversity in the indoor wireless channel," *IEEE Trans. Veh. Technol.*, vol. 40, pp. 569–574, 1991.

[16] C. F. Yang, C. J. Ko, and J. Y. Chen, "Measurement of the dielectric constants of the walls in buildings," in *Proc. 1st Radio Science Symp.*, Kaohsiung, Taiwan, 1995, pp. 63–67.

[17] M. C. Lawton and J. P. McGeehan, "The application of a deterministic ray launching algorithm for the prediction of radio channel characteristic in small-cell environments," *IEEE Trans. Veh. Technol.*, vol. 43, no. 4, pp. 966–969, 1994.

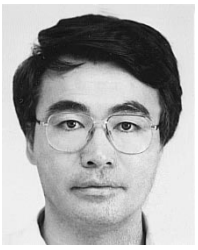

J. H. Tarng (M'89) received the B.S. degree in power mechanical engineering from National Tsin-Hua University, Hsin-Chu, Taiwan, R.O.C., in 1981 and the M.S. and Ph.D. degrees in electrical engineering from Pennsylvania State University, University Park, in 1988 and 1989, respectively.

He is currently a Faculty Member in the Department of Communication Engineering, National Chiao Tung University, Hsin-Chu. His current research interests include radio channel modeling and measurement, frequency/channel assignment, and radio electromagnetic interference.

T. R. Liu received the M.S. degree in communication engineering from National Chiao-Tung University, Hsin-Chu, Taiwan, R.O.C., in 1996.

His research interests include indoor propagation modeling and measurement.